Interaction of modified oligonucleotides with nuclear proteins, formation of novel nuclear structures and sequence-independent effects on RNA processing

Loren L Flynn #, Ruohan Li # May T Aung-Htut, Ianthe L Pitout, Jack A L Cooper, Alysia Hubbard, Lisa Griffiths, Charlie Bond, Steve D Wilton, Archa H Fox* and Sue Fletcher*

 # authors contributed equally

***corresponding authors**

Abstract (max 150 words)

Oligonucleotides and nucleic acid analogues that alter gene expression are showing therapeutic promise for selected human diseases. The modification of synthetic nucleic acids to protect against nuclease degradation and to influence drug function is common practice, however, such modifications may also confer unexpected physicochemical and biological properties. Here we report backbone-specific effects of modified oligonucleotides on subnuclear organelles, altered distribution of nuclear proteins, the appearance of novel structured nuclear inclusions, and modification of RNA processing in cultured cells transfected with antisense oligonucleotides on a phosphorothioate backbone. Phosphodiester and phosphorodiamidate morpholino oligomers elicited no such consequences. Disruption of subnuclear structures and proteins elicit severe phenotypic disturbances, revealed by transcriptomic analysis of fibroblasts exhibiting such disruption. These data suggest that the toxic effects and adverse events reported after clinical evaluation of phosphorothioate nucleic acid drugs may be mediated, at least in part, by non-specific interaction of nuclear components with the phosphorothioate backbone.

Key Words

Antisense oligonucleotides, RNA analogue, RNA processing, paraspeckle proteins, nuclear organelles

Abbreviations

antisense oligonucleotide (AO), spinal muscular atrophy (SMA), Duchenne muscular dystrophy (DMD) phosphorodiamidate morpholino oligomer (PMO) amyotrophic lateral sclerosis (ALS)

Introduction

Antisense oligonucleotide drugs are a class of therapeutics designed to alter gene expression and function, and are reported to have delivered therapeutic benefit to spinal muscular atrophy (SMA) type 1 patients (Paton 2017) and a subset of Duchenne muscular dystrophy (DMD) cases (Mendell *et al.* 2013, Mendell *et al.* 2016). *Nusinersen* (*Spinraza*) is a 2′O-methoxyethyl antisense oligonucleotide (AO) on a phosphorothioate backbone, targeting a splice silencer (*ISS-N1*) in *SMN2* intron 7 that promotes exon 7 selection during pre-mRNA splicing (Singh *et al.* 2006) and received Food and Drug Administration (USA) (FDA) approval in December 2016 for the treatment of SMA. *Exondys51* is a phosphorodiamidate morpholino oligomer (PMO) that targets the *DMD* pre-mRNA to exclude exon 51, in order to re-frame the dystrophin transcript around frame shifting deletions flanking exon 51, as a treatment for DMD (Mendell *et al.* 2013). *Exondys51* received accelerated approval from the FDA on September 19th 2016. Other drugs exploiting the antisense concept include Kynamro® (mipomersen sodium) (Wong and Goldberg 2014), an adjunctive treatment to reduce LDL-C levels in familial hypercholesteremia, approved in January 2013, followed by an FDA hepatotoxity black box warning; and a number of compounds at various stages of clinical development, predominantly siRNA and oligodeoxyribonucleotide analogues designed to induce RNAse H degradation of target transcripts (for review see (Bennett *et al*. 2017, Stein and Castanotto 2017)). Recently, Alnylam announced the first FDA approval of an RNAi Therapeutic, ONPATTRO™ (patisiran) for the treatment of adult patients with polyneuropathy of hereditary transthyretin-mediated amyloidosis. (https://www.fda.gov/NewsEvents/Newsroom/PressAnnouncements/ucm616518.htm)

Strategies to improve biological stability and confer pharmaceutical properties to nucleic acid drugs include chemical modifications of the bases and nucleic acid backbone to increase resistance to endogenous nucleases; modifications that influence specific oligomer activity and conjugates that enhance cellular uptake and improve tissue distribution. While the phosphorothioate backbone is the most widely applied chemical modification, changes to the ribose moiety (eg, 2′ O-methylation, 2′ O-methoxyethyl, 2′ O-fluoro), nucleobases and other backbone modifications, including peptide nucleic acids and phosphorodiamidate morpholino oligomers can confer specific characteristics and mechanisms of action (for review see (Veedu 2015, Wilton *et al.* 2015, Tri Le *et al.* 2016)).

Many laboratories, including our own, routinely use 2′ O-methyl phosphorothioate oligonucleotides to evaluate antisense sequences for targeted splicing modulation, and different modified bases on a phosphorothioate backbone for various other molecular interventions (Lipi *et al.* 2016, Chakravarthy *et al.* 2017). These compounds can be economically prepared in-house and efficiently transfected into a range of cells as cationic liposomes or dendrimer complexes, using commercially available reagents. However, for sustained splice modification, *in vivo* use and clinical application, PMOs have proved safe and effective (Gebski *et al.* 2003, Fletcher *et al.* 2006, Kinali *et al.* 2009, Mendell *et al.* 2016). We previously reported that antisense exon skipping sequences prepared and optimized *in vitro* as 2′ O-methyl phosphorothioate oligonucleotides generally perform comparably when synthesized as PMO (Adams *et al.* 2007). An extended antisense sequence targeting the *ISS-N1* region of *SMN2* was validated *in vitro* and *in vivo* using 2′ O-methyl phosphorothioate and PMO chemistries (Mitrpant *et al.* 2013).

Phosphorothioate backbone modification of nucleic acid drugs is common practice for protection from rapid degradation by circulating and intracellular nucleases, but these modified AOs can interact undesirably with endogenous cellular components. Early work indicated that negatively charged phosphorothioate AOs bind non-specifically to heparin-like proteins, laminin and collagen (Dias and Stein 2002) and more recently, phosphorothioate AOs were reported to interact with nuclear paraspeckle-associated proteins, sequestering them away from their endogenous target, the long non-coding RNA *NEAT1,* and also seeding paraspeckle like-structures in the absence of *NEAT1* (Shen *et al.* 2014, Shen *et al.* 2015). Paraspeckles and paraspeckle proteins are involved in transcriptional regulation, transport and splicing pathways (Bond and Fox 2009, Naganuma *et al.* 2012). Beyond the paraspeckle-associated subset (Shen *et al.* 2014), phosphorothioate AOs were also reported to bind an additional approximately 50 intracellular proteins (Liang *et al.* 2015) however, these interactions were studied in the context of evaluating the modest impact these interactions had on AO function (Liang *et al.* 2015). A broader question relates to the global consequences on cellular processes arising as a result of the interaction of AOs with nuclear proteins.

Results of *in vivo* studies investigating the consequences of non-specific phosphorothioate AO binding are particularly relevant when considering therapeutic applications. The

sequestration of paraspeckle proteins, in particular proteins of the drosophila behaviour/human splicing (DBHS) family, was associated with acute hepatotoxicity, inflammation and apoptosis after application of 2´ fluoro-modified phosphorothioate antisense oligonucleotides with a 5-10-5 gapmer configuration in mice (Shen *et al.* 2018) and while this study focused on the severity of 2´ fluoro-modified phosphorothioate AOs, all 2´ modifications evaluated have been shown to sequester paraspeckle proteins, albeit to varying degrees (Shen *et al.* 2014, Liang *et al.* 2015, Shen *et al.* 2018). The backbone-dependent binding of phosphorothioate-modified olionucleotides to platelets *in vitro* and *in vivo*, mediated by the platelet-specific receptor glycoprotein VI (GPVI) is also of note (Flierl *et al.* 2015), considering the broad range of nucleic acid therapeutics currently under investigation (for review see (Bennett *et al.* 2017). Oligonucleotides on a phosphorothioate-modified backbone elicited strong platelet activation, signaling, reactive oxygen species generation, adhesion, spreading, aggregation and thrombus formation (Flierl *et al.* 2015). Of particular relevance to current clinical usage, 2´ O-methyl phosphorothioate AOs were reported to activate innate immunity when administered directly to the central nervous system (Toonen *et al.* 2018).

Here we report that transfection of cultured cells with 2´ O-methyl phosphorothioate antisense sequences resulted in numerous novel, large nuclear inclusions in the form of highly structured fibril-like aggregates that co-stained for the paraspeckle proteins, NONO, SFPQ, PSPC1 and FUS. Other nuclear proteins showed altered distribution in 2´ O-methyl phosphorothioate transfected cells. Intranuclear inclusions begin to form within four hours of transfection, and become dominant structures throughout the nucleus within 24 hours. The inclusions appear stable once formed and may remain evident on the culture substrate, even after death and disintegration of the cell. Transmission electron microscopy on transfected cells revealed numerous large, regular structures reminiscent of amyloid deposits, with electron dense regions. Furthermore, gene ontology analyses following RNA sequencing demonstrated significant disruptions to chromatin silencing; regulation of autophagy; nucleotide excision repair; membrane and organelle organization; apoptosis; signalling and protein transmembrane transport, following 2´ O-methyl phosphorothioate transfection.

Materials and Methods

136 *Antisense oligonucleotides*
137 Phosphorodiamidate morpholino oligomers (PMOs) were purchased from Gene-Tools LLC
138 (Philomath, OR, USA), and 2′ O-methyl phosphorothioate AOs were synthesised by TriLink
139 BioTechnologies (San Diego CA, USA). The following sequences were evaluated; an AO
140 encompassing the *SMN* intron 7 *ISS-N1* target, but with a longer sequence *SMN7D(-10-29)*
141 (5′AUUCACUUUCAUAAUGCUGG 3′); the Gene-Tools standard control oligomer, only
142 known to be biologically active in reticulocytes carrying a splice mutation in the human beta-
143 globin pre-mRNA, as an unrelated sham control AO sequence
144 (5′CCUCUUACCUCAGUUACAAUUUAUA 3′), and identified as 'control AO' throughout
145 this study; *Smn* (5′CAC CUU CCU UCU UUU UGA UU 3′) designed to induce exon mouse
146 *Smn* exon skipping and a *SMN* sense AO (5′ CCAGCAUUAUGAAAGUGAAU 3′)
147 complementary to *SMN7D(-10-29)*.
148
149 *Transfection*
150 The 2′O-methyl phosphorothioate AOs were transfected into dermal fibroblasts as lipoplexes
151 using 3 µl of Lipofectamine 3000 (Life Technologies, Melbourne, Australia) per 1 ml of
152 OptiMEM, according to the manufacturer's protocol. The transfection mix was applied to
153 cells seeded at 10,000 per cover slip for immunofluorescence and 15,000 cells per well in 24
154 well plates for RNA extraction and incubated (37°C) for 24 hours prior to RNA and protein
155 analysis. SMA patient fibroblasts were used for the experiments shown in Figures 1f and 1g
156 (Coriell Cell Repositories, GM03813) and fibroblasts from our in-house biobank, obtained
157 from a healthy volunteer, with informed consent (Murdoch University Human Research
158 Ethics Committee Approval #2013/156) were used for all other experiments, except live-cell
159 imaging (see below).
160
161 PMOs were delivered to cells either uncomplexed (10 µM), annealed to a complementary
162 sense DNA oligonucleotide (phosphodiester leash) and transfected as a lipoplex (200 nM), or
163 by nucleofection using a Nucleofector™ X Unit (Lonza, Melbourne, Australia) according to
164 the manufacturer's instructions. PMOs were delivered using the P2 nucleofection kit and CA-
165 137 program at 1 µM, as determined by the final transfection volume. All PMO transfections
166 were incubated for 72 hours prior to RNA and protein analysis.
167
168 *RT-PCR on AO transfected cells*
169 RNA was extracted using the MagMAX-96 Total RNA Isolation Kit, including DNase

170 treatment (Life Technologies), according to the manufacturer's instructions. RT-PCRs were
171 performed using the One-step Superscript III RT-PCR kit with Platinum Taq polymerase (Life
172 Technologies) according to the manufacturer's instructions. All primer sequences and PCR
173 conditions used in this study are detailed in Supplementary File 1**, Table 1**.
174
175 *cDNA synthesis and quantitative PCR*
176 cDNA was synthesised from (~500 ng) RNA extracted from treated and untreated cell cultures
177 using the Superscript IV first-strand synthesis system (Life Technologies) as per the
178 manufacturer's instructions. Prior to qPCR amplification, cDNA was diluted in RNase/DNase
179 free water (1:5).
180
181 The qPCR reactions were performed using Fast SYBR™ Green Master Mix (ThermoFisher
182 Scientific, Melbourne, Australia) and primers for ribosomal RNA subunits *5S* (100% primer
183 efficiency), *18S* (95% primer efficiency), *45S* (100% primer efficiency) and housekeeping Tata
184 box protein (*TBP;*100% primer efficiency) and beta Tubulin (*TUBB;*94% primer efficiency)
185 transcripts. All primer sequences and cycling conditions used in this study are detailed in
186 Supplementary File 1, **Table 1.** Transcript abundance was measured using the CFX384 Touch™
187 Real Time PCR detection system (Bio-Rad Laboratories Pty., Ltd., Gladesville, Australia). The
188 relative expression of each ribosomal RNA subunit to *TBP* and *TUBB* mRNA was calculated
189 using the $2^{-\Delta\Delta CT}$ method and presented as a fold change compared to untreated cells.
190
191 *Immunofluorescence*
192
193 Approximately 10,000 fibroblasts were seeded onto 22 mm x 22 mm coverslips in
194 6-well plates and incubated for 24 hours, prior to transfection. Following transfection,
195 the cells were fixed using acetone:methanol (1:1) on ice for 4 minutes and air-dried.
196
197
198 Fixed cells were washed in PBS containing 1% Triton X-100 to permeabilise the
199 nuclear membrane, and then in PBS to remove excess Triton X-100. Primary antibodies
200 were diluted in PBS containing 0.05% Tween20 and applied to cells for 1 hour at room
201 temperature. All antibody details and staining conditions are listed in Supplementary File
202 1 **Table 2**. Primary antibodies were detected using AlexaFluor488 anti-mouse (cat no.
203 A11001), anti-rabbit (cat. No A11008) or AlexaFluor568 anti-mouse (cat. No A11004) or
204 anti-rabbit (cat. No A11011) (1:400) after incubation for 1 hour at room temperature, and

205 counterstained with Hoechst 33342 (Sigma-Aldrich) for nuclei detection (1 mg/ml, diluted
206 1:125).
207
208 *Western blotting*
209 Cell lysates were prepared with 125 mM Tris/HCl pH 6.8, 15% SDS, 10% Glycerol, 1.25 µM
210 PMSF (Sigma-Aldrich, NSW, Australia and 1x protease inhibitor cocktail (Sigma-Aldrich)
211 and sonicated 6 times (1 second pulses) before adding bromophenol blue (0.004%) and
212 dithiothreitol (2.5 mM). Samples were heated at 94°C for 5 minutes, cooled on ice and
213 centrifuged at 14,000 x g for 2 min before loading onto the gel.
214
215 Total protein (10 µg), measured by BCA, was loaded per sample on a NuPAGE Novex 4-12%
216 BIS/Tris gel (Life Technologies) and separated at 200 V for 55 minutes. Proteins were
217 transferred onto a Pall Fluorotrans polyvinylidene fluoride (PVDF) membrane at 350 mA for
218 2 hours. Following blocking for 1 hour, the membrane was incubated in 5% skim milk
219 powder in 1x TBST containing the primary antibody diluted as shown in Supplementary File
220 1, **Table 2.** Immunodetection was performed using the Western Breeze Chemiluminescent
221 Immunodetection System (Life Technologies) according to the manufacturer's instructions.
222 Western blot images were captured on a Vilber Lourmat Fusion FX system using Fusion
223 software and Bio- 1D software was used for image analysis.
224
225
226 *Live cell imaging*
227 U2OS cells, previously modified to tag the endogenous SFPQ gene with GFP were used for
228 live-cell imaging (Li *et al.* 2017). Cells were seeded at 1.5 x 10^5 cells per well in a 12-well
229 plate, 24 hours before transfection, with high glucose DMEM (Life Technologies, Cat
230 No.11995065) supplemented with 10% fetal calf serum and 1% penicillin-streptomycin. On
231 the following day, cells in each well were transfected with 100 nM 2´ O-methyl
232 phosphorothioate AOs complexed with 2.2 µl Lipofectamine 3000 following the
233 manufacturer's instructions. Immediately after transfection, the plate was transferred to an
234 Incucyte S3 (Essen Bioscience) for live-cell imaging at 1 hour intervals under 10 x optical
235 zoom. SFPQ-GFP and activated caspase-3/7 were visualised under standard green and red
236 channels. Incucyte Caspase-3/7 Red Apoptosis Assay Reagent (Essen Bioscience, Cat No.
237 4704) was used to reveal cell apoptosis events.
238

239 *High resolution microscopy*
240 SIM imaging was performed using an N-SIM microscope (Nikon Corporation, Tokyo, Japan),
241 with SR Apochromat TIRF 100 x 1.49 NA oil immersion objective. Spherical aberration was
242 reduced using the Ti2 automated correction collar at the beginning of the imaging session.
243 Images were acquired using 405 nm, 488 nm and 561 nm lasers, with stacks of step size 0.12
244 µm (with top and bottom of samples determined visually), using 3D-SIM mode. Images were
245 reconstructed with NIS Elements software (Nikon Corporation, Tokyo, Japan).
246
247 *Transmission electron microscopy*
248 Following transfection, cells were washed in PBS and fixed in cold 2.5% phosphate buffered
249 glutaraldehyde overnight. The fixed cells were scraped and centrifuged, then embedded in 4%
250 agarose. The pellets were processed using a Leica tissue processor, moving through 1%
251 aqueous osmium tetroxide, increasing graded alcohols, propylene oxide, propylene
252 oxide/araldite mix, and finally pure araldite resin. The osmicated cells, surrounded by resin in
253 a beem capsule were polymerised overnight at 80°C to form hard blocks.
254 Semi-thin (0.5 micron) sections were taken from the blocks using glass knives, on an RMC
255 ultratome, and stained with methylene blue (0.1% aqueous Methylene Blue with 0.1%
256 Borax) to visualise available cells. Ultrathin sections were then cut from selected blocks,
257 using a Diatome diamond knife, at approximately 95 nm thickness and mounted on copper
258 mesh grids and stained with uranyl acetate (5% uranyl acetate solution in 5% aqueous acetic
259 acid) and Reynold's lead citrate. The grids were viewed using a JEOL 1400 TEM, at 80 kV
260 and images captured by an 11-megapixel GATAN digital camera at varying magnifications.
261
262 *RNA sequencing and analysis*
263 RNA quality was confirmed using a Bioanalyser (Perkin Elmar, MA, USA) prior to
264 RNAseq. Samples were sent to the Australian Genome Research Facility (AGRF, Perth and
265 Melbourne, Australia) for whole transcriptome library preparation using the TruSeq Stranded
266 Total RNA Library Prep Kit (Illumina, CA, USA) and ribosomal RNA depletion with the
267 Ribo-Zero-Gold kit (Illumina, CA, USA). Sequencing was performed using an Illumina
268 HiSeq 2500 (Illumina, CA, USA) to generate 100 base pair single end reads, resulting in an
269 average 25 million reads per sample. Raw sequencing files were quality checked using
270 FastQC (0.11.7), with all files passing. No adapter contamination was identified, and reads
271 were not trimmed. Transcript quantification was performed with salmon (0.8.2), using an
272 index constructed from the Ensembl GRCh38.93 annotation. Transcript abundance was

273 summarised to gene-level counts and imported into R using tximport (1.4.0). Differential
274 expression analysis was performed using DESeq2 (1.16.1) and the default parameters (alpha
275 = 0.1). The heatmap of differentially expressed genes ($p_{adj} < 0.1$) was constructed using the
276 heatmap.2 function from R package gplots (3.0.1). Gene ontology analysis was performed
277 using GSEA (3.0) with 1000 gene set permutations. The gene ontology network was
278 constructed using the Enrichment Map plugin for Cytoscape (3.5.1), with cut-offs: $p < 0.05$,
279 FDR < 0.1 and edge > 0.3.
280
281 **Results**
282
283 *Formation of nuclear inclusions after 2´ O-methyl phosphorothioate AO transfection*
284 The phosphorothioate backbone can interact non-specifically with both intra- and extra-
285 cellular proteins, and recruits paraspeckle proteins and forms paraspeckle-like structures
286 when transfected into Hela cells (Shen *et al.* 2014). However, the dynamics of the formation
287 of these structures, as well as the long-term consequences of these structures on cell
288 physiology remain unknown.
289
290 In this study, we largely focused on two 2´ O-methyl phosphorothioate AOs, one that
291 promotes *SMN2* exon 7 retention during splicing by targeting the *ISS-N1* intronic silencer
292 motif (Singh *et al.* 2006) and the other a control oligomer sequence reported by Genetools
293 LLC and widely used as a transfection control, although additional AO sequences were also
294 tested in some experiments, as indicated below. In order to follow nuclear inclusion
295 formation, we first transfected 2´ O-methyl phosphorothioate AO as lipoplexes (100 nM)
296 into U2OS cells expressing genome engineered GFP-labelled endogenous SFPQ (Li *et al.*
297 2017) and performed live cell imaging over 48 hours (**Figure 1a**). The AO transfection
298 induced formation of nuclear inclusions within 5 hours, and over a period of 12 hours, all of
299 the SFPQ within the nucleus is observed sequestered within the inclusions, as revealed by
300 decreased SFPQ staining of the nucleoplasm. Ultimately, only the inclusions are evident, at
301 which time, the inclusions then coalesce into discrete filaments.
302
303 Immunofluorescent staining of the paraspeckle protein, NONO, showed colocalization in
304 nuclear inclusions in fibroblasts transfected with 2´ O-methyl phosphorothioate *SMN7D(-10-*
305 *29)* sequence at 100 nM concentration, but were also evident at AO concentrations as low as
306 12.5 nM within 24 hours of transfection (**Figure 1b**). Of note, the untreated cells show

307 diffuse nucleoplasmic NONO signal, as well as naturally occurring punctate NONO inside
308 endogenous paraspeckle nuclear bodies (Fox *et al.* 2018) (eg. **Figure 1b** (ii)). Nuclear
309 inclusions were also observed following 2′O-methyl phosphorothioate AO transfection into
310 normal human myoblasts, transformed mouse *H2K* myoblasts, and the neuroblastoma SH-
311 SY5Y cell line (Supplementary File 1, **Figure 1).** Once formed, the inclusions appear to be
312 highly stable, and remain evident on the culture substrate following cell death and nuclear
313 fragmentation and blebbing **(Figure 1c (i-ii)).** The nuclear inclusions appear as either long
314 'filaments', punctate foci, or both (**Figure 1c (iii)**). In the past we have routinely observed
315 marked cell death associated with transfection of 2′ O-methyl phosphorothioate AOs into
316 primary cells and cell lines, and hence explored any correlation between cell death and the
317 formation of AO-induced nuclear inclusions. Indeed, we observed here that transfection with
318 2′ O-methyl phosphorothioate AO sequences induced nuclear inclusions that correlated with
319 reduced cell survival (**Figure 1d-e**).
320
321 While transfection of AOs with phosphorothioate and phosphodiester backbones have been
322 demonstrated to result in nuclear inclusions (Shen *et al.* 2014), PMOs are yet to be evaluated
323 in this context. We therefore transfected fibroblasts with the AO sequences described above,
324 synthesized as PMOs. Transfection of the PMO sequences into fibroblasts did not alter the
325 apparent distribution of NONO, nor of any other nuclear proteins studied (**Figure 1f).** In
326 order to demonstrate that poor cellular uptake of these compounds was not a factor, PMOs
327 were transfected using three established delivery techniques known to lead to altered target
328 gene expression; uncomplexed PMO (10 μM), nucleofection (1 μM), and annealed to a
329 complementary DNA "leash" and transfected as a lipoplex (200 nM), all incubated for 72
330 hours after transfection (**Figure 1f (i-iii),** respectively). Immunofluorescent detection of
331 NONO showed no PMO-induced intranuclear inclusion formation or altered distribution of
332 NONO following transfection, under any of the conditions used, and was reproducible,
333 irrespective of the PMO sequence. Transfection efficiency and altered exon selection in the
334 target *SMN2* transcript was assessed by RT-PCR across *SMN* exons 4-8, confirming that the
335 absence of intranuclear inclusions in PMO transfected cells was not a consequence of poor
336 uptake of PMO (**Figure 1g**).
337
338
339
340

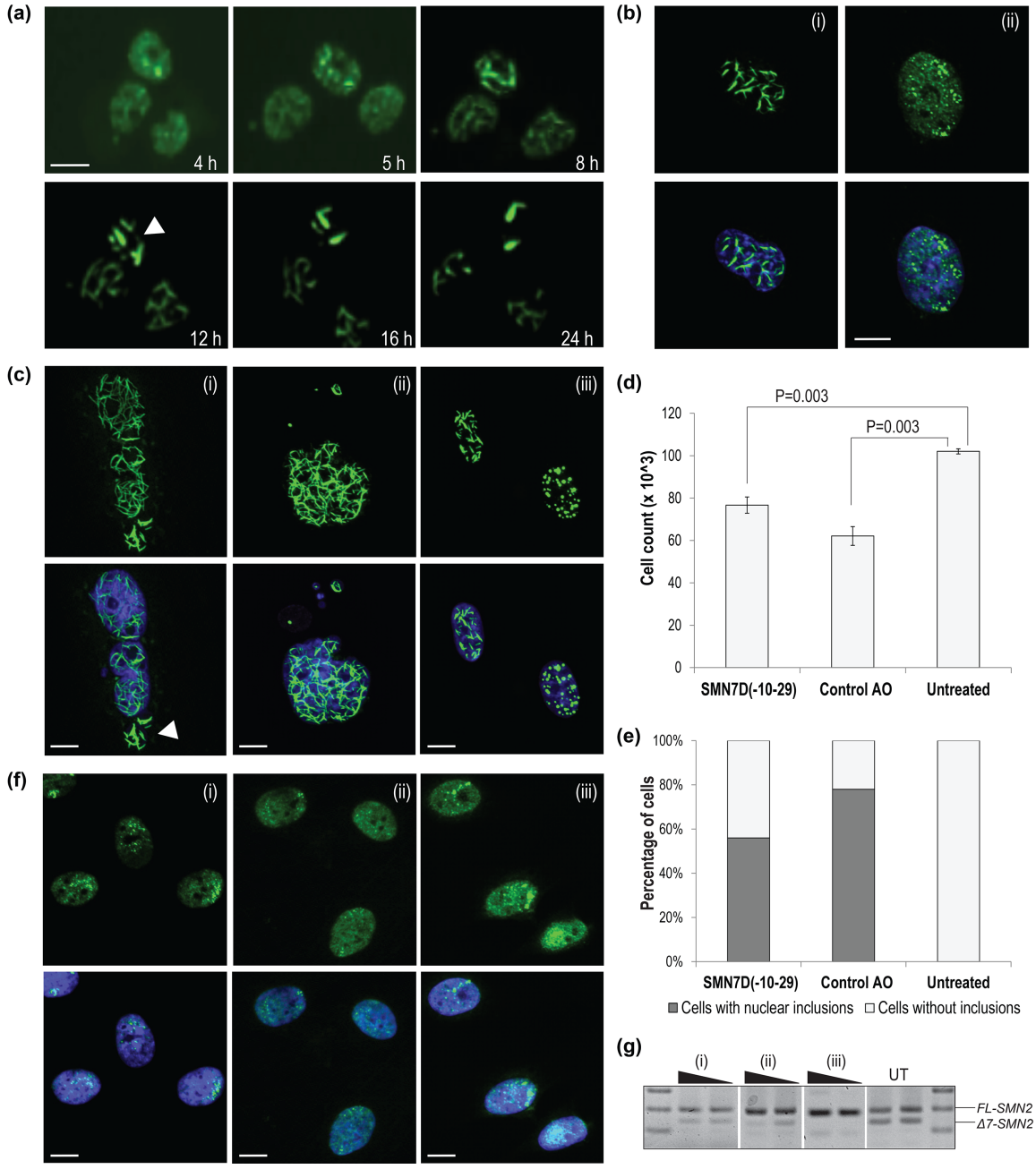

Figure 1 – Formation of nuclear inclusions. Showing **(a)** live cell imaging time-course of U2OS cells with endogenous SFPQ-GFP showing the formation of nuclear inclusions over 24 hours following 2´ O-methyl phosphorothioate control AO transfection (100 nM), inclusions are indicated by the white arrow; **(b)** fibroblasts transfected with 12.5 nM of 2´ O-methyl phosphorothioate *SMN7D(-10-29)* stained for NONO (i), compared to untreated fibroblasts (ii); **(c)** fibroblasts stained for NONO show, (i) nuclear inclusions without evidence of nuclear staining after 2´ O-methyl phosphorothioate *SMN7D(-10-29)* transfection, (ii) nuclear blebbing after 2´ O-methyl phosphorothioate control AO transfection and (iii) nuclear inclusions in the form of filaments or foci induced by transfection with a 2´ O-methyl phosphorothioate *SMN7D(-10-29)* sense sequence AO; **(d)** graph showing the number of viable fibroblasts following 2´ O-methyl phosphorothioate AO transfection (n=4), error bars represent standard error of the mean and P-values were calculated using an unpaired T-test; **(e)** graph showing the percentage of fibroblasts containing nuclear inclusions following 2´ O-methyl phosphorothioate transfection with a minimum of 200 cells counted per sample; **(f)** fibroblasts stained for NONO after transfection with PMO *SMN7D(-*

355 *10-29)* at (i) high dose un-complexed (10 µM), (ii) using a complementary leash and transfection reagent (200
356 nM) and (iii) using electroporation (1 µM), all incubated for 72 hours; and **(g)** RT-PCR of full length (FL) and exon
357 7 skipped (Δ7) *SMN2* transcripts of RNA collected following transfections as in **(f)**. All scale bars = 10 µm.
358

359 To further explore whether AO-induced nuclear inclusions are sequence independent, ninety
360 2′ O-methyl phosphorothioate AOs targeting structural gene transcripts, transcription factors,
361 splicing factors and enzymes, were transfected into fibroblasts and the cells were
362 immunostained for SFPQ (Supplementary File 1, **Table 3)**. All AOs tested disrupted SFPQ
363 distribution and all but one AO formed nuclear inclusions by 24 hours following AO
364 transfection at 100 nM, irrespective of length (18-30 bases) and nucleotide composition
365 (Supplementary File 1, **Table 3**), indicating that with optimal transfection efficiency, any 2′
366 O-methyl phosphorothioate sequence is likely to induce nuclear inclusions. One transfected
367 AO induced NONO localization to the nuclear envelope (Supplementary File 1, **Figure 2a**),
368 while a number of AO sequences induced cytoplasmic SFPQ aggregates in addition to
369 nuclear inclusions (Supplementary File 1, **Figure 2b**). The AO-mediated cytoplasmic
370 aggregate formation was also reported by Liang *et al.,* 2014, who observed cytoplasmic
371 structures as a consequence of TCP1-beta subunit interaction with phosphorothioate-AOs in
372 the cytoplasm, in addition to formation of nuclear 'phosphorothioate bodies', and concluded
373 that upon transfection, the TCP1 proteins interact with phosphorothioate AOs and enhance
374 antisense activity (in this case, activation of the RNase H-mediated target degradation)
375 (Liang *et al.* 2015).

376
377 *Composition of nuclear inclusions induced by 2′ O-methyl phosphorothioate AO transfection*
378 The structure and composition of nuclear inclusions was further investigated by
379 immunostaining of additional selected nuclear proteins found in paraspeckles, the nuclear
380 envelope, nucleoli, nuclear speckles, Cajal bodies and nuclear stress bodies. The paraspeckle
381 proteins PSPC1 and FUS were evident in nuclear inclusions (Supplementary File 1, **Figure**
382 **3a and 3b)** while the proteins TDP-43 and hnRNP-A1 were not observed to be components
383 of nuclear inclusions (Supplementary File 1, **Figure 3c and 3d).**
384

385 Coilin, a component of nuclear Cajal bodies, shows altered distribution in 2′ O-methyl
386 phosphorothioate control AO transfected cells and is distributed evenly through the
387 nucleoplasm and cytoplasm of transfected cells showing NONO-positive nuclear inclusions,
388

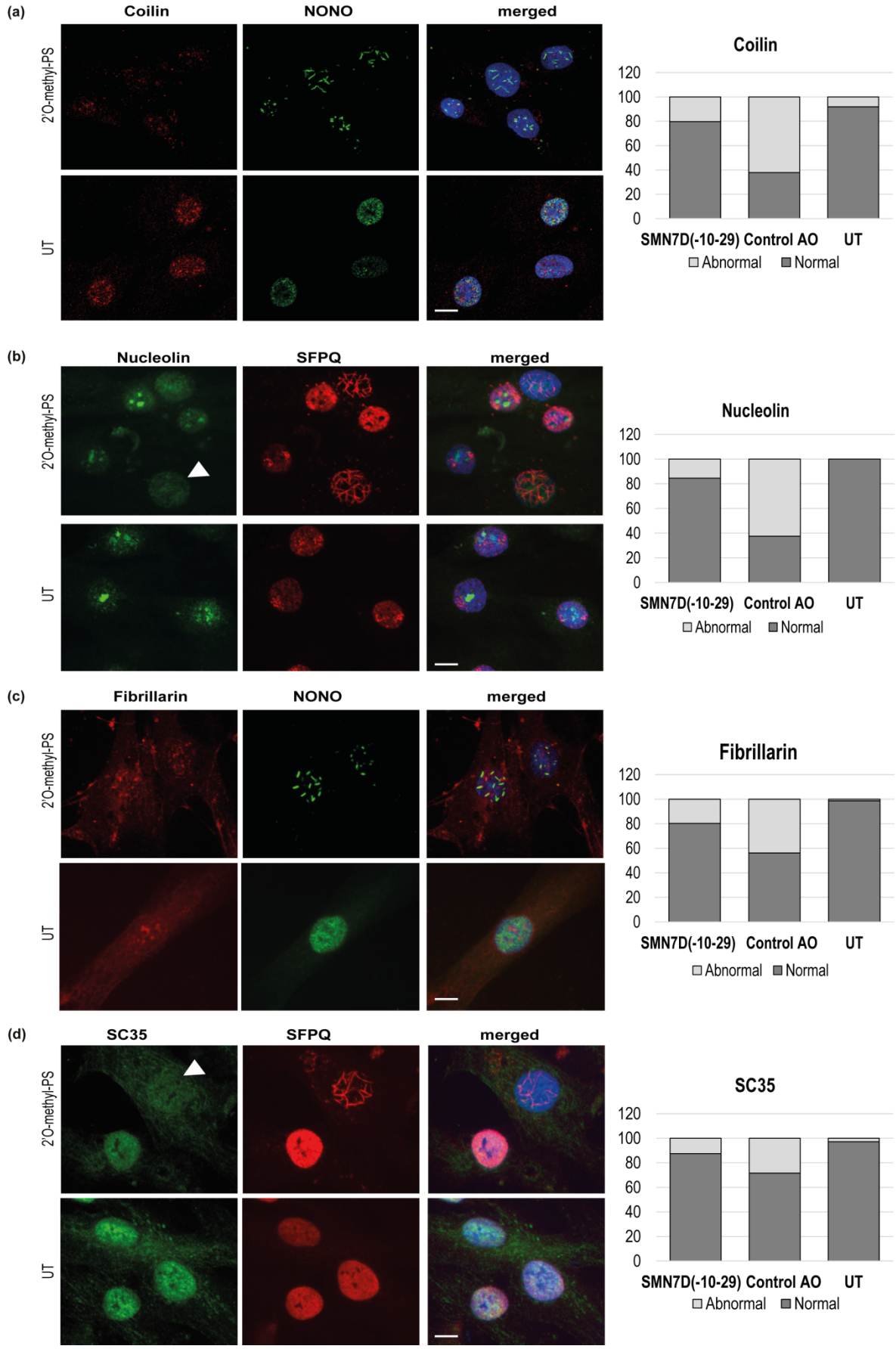
(a)
Coilin
NONO
merged
2'O-methyl-PS
UT
Coilin
120
100
80
60
40
20
0
SMN7D(-10-29)
Control AO
UT
Abnormal
Normal
(b)
Nucleolin
SFPQ
merged
2'O-methyl-PS
UT
Nucleolin
120
100
80
60
40
20
0
SMN7D(-10-29)
Control AO
UT
Abnormal
Normal
(c)
Fibrillarin
NONO
merged
2'O-methyl-PS
UT
Fibrillarin
120
100
80
60
40
20
0
SMN7D(-10-29)
Control AO
UT
Abnormal
Normal
(d)
SC35
SFPQ
merged
2'O-methyl-PS
UT
SC35
120
100
80
60
40
20
0
SMN7D(-10-29)
Control AO
UT
Abnormal
Normal

389

390 **Figure 2 – Staining of nuclear bodies following 2´ O-methyl phosphorothioate transfection (100 nM, 24**
391 **hours), with AOs as indicated in fibroblasts**. **(a)** transfected with the control AO showing coilin (red) and
392 NONO (green) overlayed with hoechst (blue), and graph showing the percentage of abnormal and normally
393 stained cells in cultures transfected with *SMN7D(-10-29)* and control AOs; **(b)** transfected with *SMN7D(-10-29)*
394 showing nucleolin (green) and SFPQ (red) overlayed with hoechst (blue), and graph showing the percentage of
395 abnormal and normally stained cells in cultures transfected with *SMN7D(-10-29)* and control AOs*;* **(c)** transfected
396 with the control AO showing fibrillarin (red) and NONO (green) overlayed with hoechst (blue), and graph showing
397 the percentage of abnormal and normally stained cells in cultures transfected with with *SMN7D(-10-29)* and
398 control AOs and **(d)** transfected with *SMN7D(-10-29)* showing SC35 (green) and SFPQ (red) overlayed with
399 hoechst (blue), and graph showing the percentage of abnormal and normally stained cell in cultures transfected
400 with *SMN7D(-10-29)* and control AOs. A minimum of 100 cells were counted for each sample. All scale bars = 10
401 µm.
402
403 whereas it is present almost exclusively in the nucleus of untreated cells (**Figure 2a).**
404 Nucleolin and fibrillarin, both markers for the nucleolus, show altered distribution in nuclear
405 inclusion-containing cells, changing from nucleolar to diffuse nucleoplasmic, as shown in
406 **Figures 2b** and **2c**, respectively. The splicing factor and component of nuclear speckles,
407 SC35, showed enhanced cytoplasmic localisation in cells that also contained nuclear
408 inclusions, revealed here by SFPQ immunofluorescence (**Figure 2d**).
409
410 The percentage of AO transfected cells showing disrupted staining or abnormal localization
411 of coilin, nucleolin, fibrillarin and SC35 staining correlated with cells containing
412 intranuclear inclusions, as indicated in the graphs (**Figure 2a-d**). Line intensity profiling
413 shows altered distribution of these nuclear proteins in individual cells that have nuclear
414 inclusions, and is presented in Supplementary File 1, **Figure 4.** Since components of
415 subnuclear organelles were disorganised following transfection with phosphorothioate AOs,
416 the levels of these proteins in the transfected cells were investigated. Western blot analysis
417 showed that the overall abundance of each protein studied to be essentially unchanged
418 following AO transfection. Representative western blots probed for SFPQ, NONO, TDP43,
419 hnRNP-A1, NCL, HSF1 and beta actin, are shown in Supplementary File 1, **Figure 5**.
420
421 *Morphology of 2´ O-methyl phosphorothioate AO-induced nuclear inclusions*
422 Detailed analysis of the 2′ O-methyl phosphorothioate *SMN7D(-10-29)*AO-induced nuclear
423 inclusions was performed using transmission electron microscopy (TEM) on ultra-thin,
424 osmium stained sections (**Figure 3a(i-vi))**. The nuclear inclusions appeared to be
425 microfibrillar or amyloid-like, approximately 200-250 nm in diameter, occurring mostly in
426 groups or bundles. For reference, the width of a DNA double helix is ~2 nm. If captured in a

427 suitable plane of section, the structures appear to have very electron dense termini. Such
428 nuclear inclusions have never before been revealed by transmission electron microscopy in
429 the investigating laboratory. The electron dense regions are reminiscent of perichromatin in
430 size and electron density, the inclusions revealed by TEM extend to ~ 2000 nm in length.
431 Numerous small, partially formed inclusions are also evident in nuclei of transfected cells
432 when viewed at higher magnification (**Figure 3a (iii)**).
433
434 Since transmission electron microscopy can only capture segments of the presumed large
435 fibril-like nuclear inclusions, super resolution microscopy was used to examine 2´ O-methyl
436 phosphorothioate *SMN7D(-10-29)* AO transfected and untreated fibroblasts (**Figure 3b-c**).
437 AO transfected fibroblasts co-stained for NONO and SFPQ show a network of many nuclear
438 inclusions characterised by co-localisation of the two proteins, whereas the untreated cells
439 show more even, punctate distribution within paraspeckles (**Figure 3b (i, ii),** respectively).
440 Transfected fibroblasts co-stained for SFPQ and FUS reveal large interconnected fibril-like
441 structures decorated with FUS at mid-points and at the termini (**Figure 3c (i)**). SFPQ, NONO
442 and FUS are all sequestered to the nuclear inclusions, unlike the even nuclear distribution of
443 these proteins in untreated cells (**Figure 3c (ii)**).
444
445 The nuclear envelope protein, lamin B1 showed altered distribution in a proportion of 2´ O-
446 methyl phosphorothioate *SMN7D(-10-29)* transfected cells that exhibited nuclear inclusions
447 (**Figure 3d (i-ii)**). In these cells, the nuclear envelope labelled by immunostaining of lamin
448 B1 appears multi lobular and distorted, reminiscent of those found in the premature ageing
449 disease progeria and in E145K cells (Taimen *et al.* 2009). A single z-frame image is shown
450 in **Figure 3d (i)** that clearly illustrates lamin B1 localized in 4 distinct nuclear lobules.
451 **Figure 3d (ii and iii)** shows the composite image and an image of an immunostained,
452 untreated fibroblast. In all images (**Figure 3b-d**), the nuclear inclusions appear to reside
453 between areas that may reflect chromosomal territories.

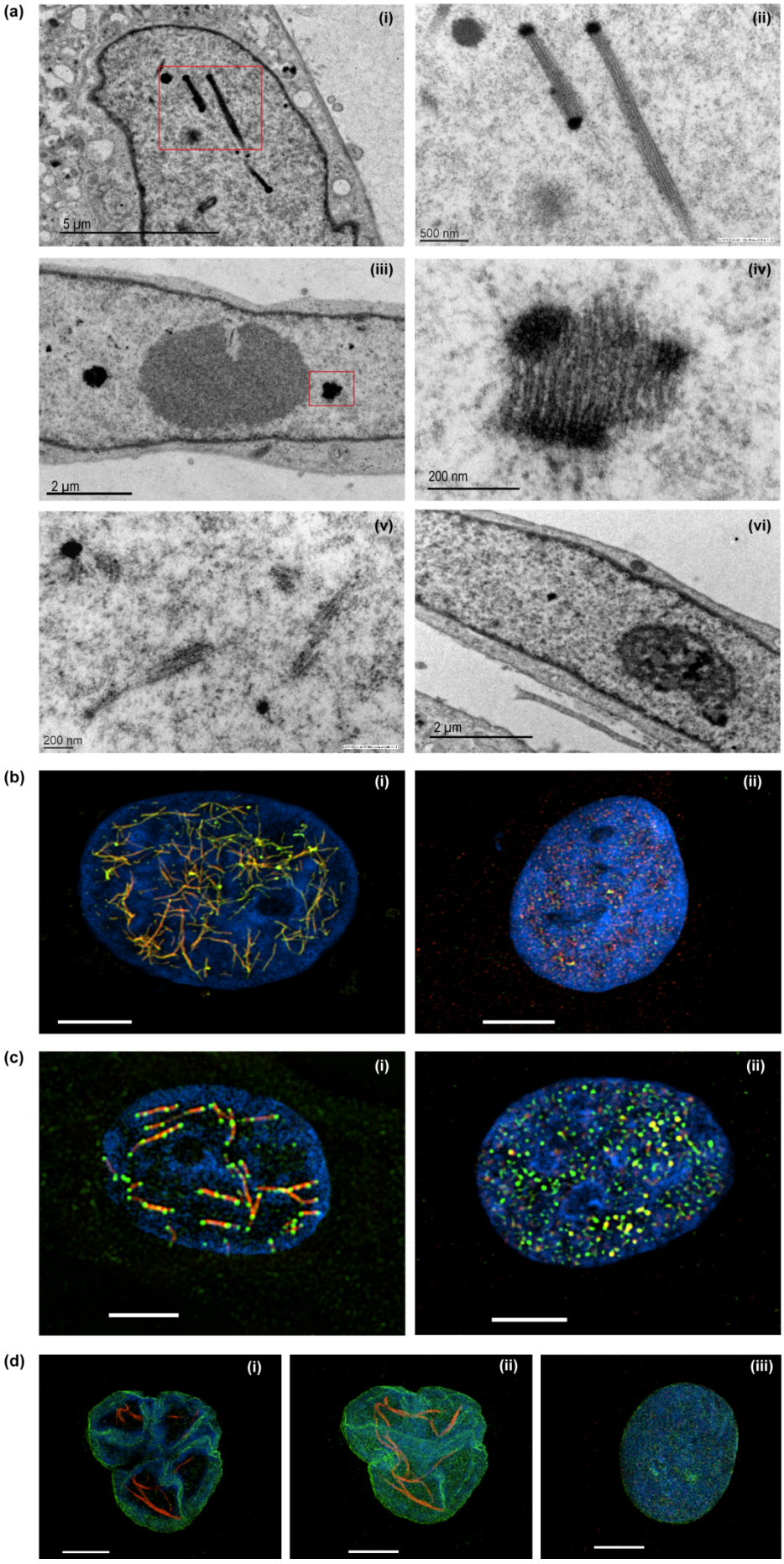
(a)
(i)
5 µm
(ii)
500 nm
(iii)
2 µm
(iv)
200 nm
(v)
200 nm
(vi)
2 µm
(b)
(i)
(ii)
(c)
(i)
(ii)
(d)
(i)
(ii)
(iii)

454

455 **Figure 3 – Structural analysis of nuclear inclusions in 2´ O-methyl phosphorothioate transfected**
456 **fibroblasts.** Fibroblasts were transfected with the 2´ O-methyl phosphorothioate AO, *SMN7D(-10-29)* at 100 nM,
457 for 24 hours). Transfected and untreated control cells were processed for transmission electron microscopy (**a**)
458 and super resolution fluorescence microscopy (**b-d**). Showing **(a)** transmission electron microscopy of (i) nucleus
459 with filament-like nuclear inclusions (scale = 5 µm), (ii) higher magnification of (i) (scale = 500 nm), (iii) nucleus
460 with foci-like nuclear inclusions (scale = 2 µm), (iv) higher magnification of (iv) (scale = 200 nm), (v) partially
461 formed nuclear inclusions (scale = 200 nm), and (vi) untreated nucleus (scale = 2 µm); **(b)** super resolution
462 fluorescence microscopy of SFPQ (green) and NONO (red) co-staining following 2´ O-methyl phosphorothioate
463 (*SMN7D(-10-29))* transfection (i) and an untreated cell (ii); **(c)** super resolution fluorescence microscopy of SFPQ
464 (red) and FUS (green) co-staining following transfection (i) and an untreated cell (ii); **(d)** super resolution
465 fluorescence microscopy of NONO (red) and LAMIN-B1 (green) co-staining following transfection (i-ii) and an
466 untreated cell (iii). A single z-frame is shown in (i) and a maximum intensity z-stack in (ii). For all SIM images
467 scale bar = 5 µm.
468

469 *2´ O-methyl phosphorothioate AOs affect ribosomal RNA processing and maturation*

470 Since Cajal bodies and fibrillarin are important in ribosomal RNA processing and assembly,
471 we assessed rRNA levels in 2´ O-methyl phosphorothioate AO transfected cells and
472 untreated cells. qPCR and bioanalyser data show unprocessed rRNA was markedly increased
473 by 2´ O-methyl phosphorothioate AO transfection in fibroblasts (**Figure 4**). A Bioanalyser
474 RNA trace from 2´ O-methyl phosphorothioate control AO transfected fibroblasts (**Figure**
475 **4a**) showed low levels of 18S and 28S ribosomal subunits, as well as a number of
476 intermediate peaks compared to that on RNA from untreated fibroblasts (**Figure 4b**),
477 consistent with incomplete rRNA processing. Poor RNA quality was ruled out, given a
478 similar pattern was observed in all experimental repeats (n=6). This observation was
479 supported by qPCR analysis of rRNA levels showing a 2 to 3.5-fold increase in the level of
480 the unprocessed 45S rRNA in 2´ O-methyl phosphorothioate transfected compared to
481 untreated fibroblasts (**Figure 4c**). Unprocessed rRNA accumulated over time, following the
482 formation of nuclear inclusions (**Figure 4d**).

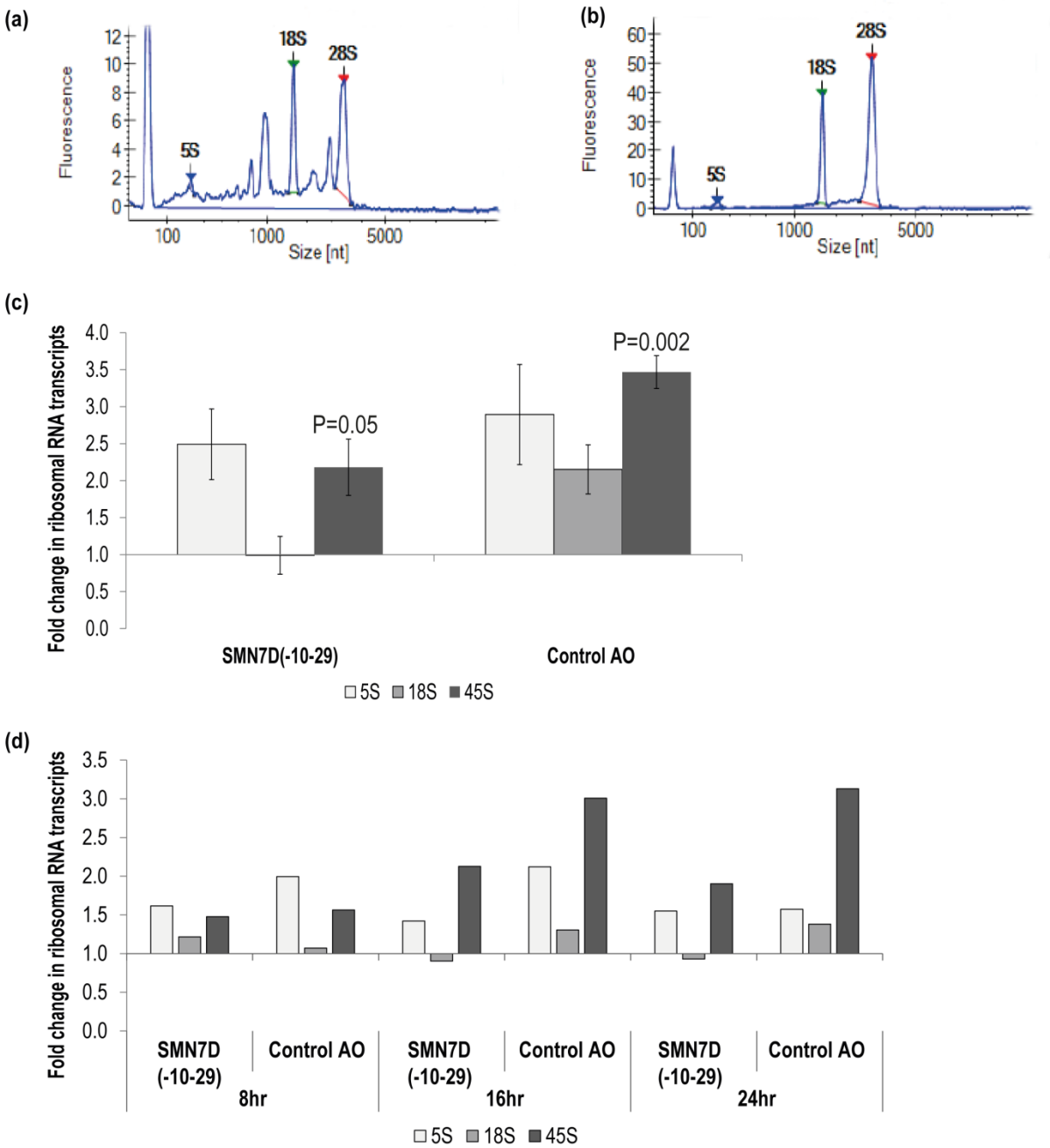

Figure 4 – Analysis of ribosomal RNA processing. Showing bioanalyser trace of rRNA from **(a)** 2´ O-methyl phosphorothioate control AO transfected cells, and **(b)** untreated cells; **(c)** qPCR analysis of 5S, 18S and 45S rRNA levels following 2´ O-methyl phosphorothioate transfection (24 hours). rRNA levels were normalised against *TBP* and compared to those in untreated cells where untreated = 1 (n=3). Error bars represent the standard error of the mean, and P-values were calculated comparing each AO treatment group to the untreated group using an unpaired T-test; and **(d)** qPCR analysis of rRNA levels over 8, 16 and 24 hours; analysis as in **(c)** (n=1).

2´ O-methyl phosphorothioate AO transfection promotes apoptosis

Following phosphorothioate AO transfection of U2OS cells at 100 nM, live cell imaging was undertaken to evaluate caspase activation (**Figure 5a**). Nuclear inclusions were observed

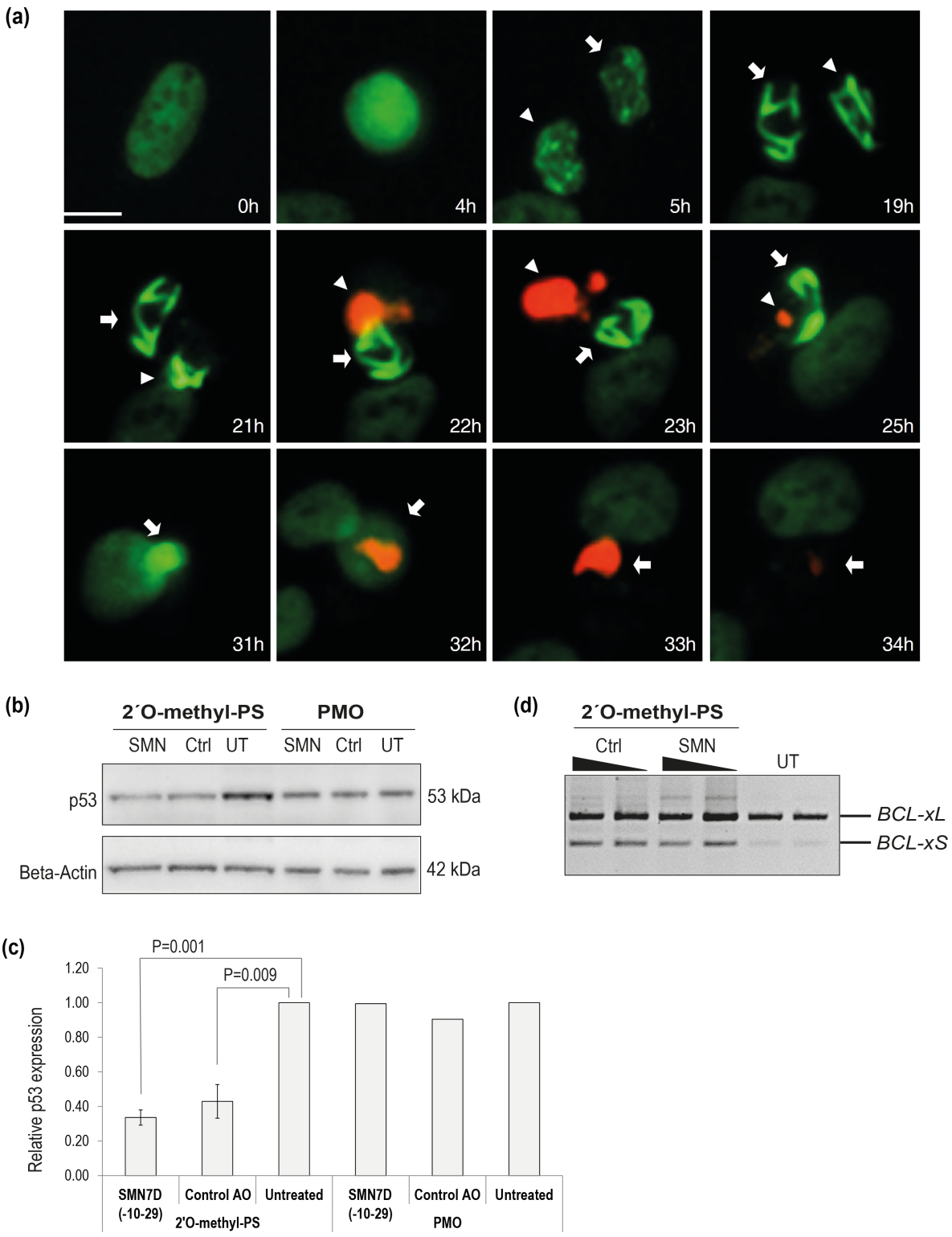

Figure 5 – Analysis of cellular toxicity following 2´ O-methyl phosphorothioate AO transfection. (a) live cell imaging over time of U2OS cells with endogenous SFPQ-GFP (green) transfected with the 2´ O-methyl phosphorothioate control AO and stained for caspase 3/7 activation (red). Two sister cells are annotated with arrows, and scale bar = 10 µm; **(b)** western blot of P53 and β-actin levels in fibroblasts following 2´ O-methyl phosphorothioate AO (n=3) and PMO transfection (n=1); **(c)** densitometry analysis of **(b)** where P53 levels are normalized to β-actin and compared to those in untreated cells where untreated = 1. Error bars represent the standard error of the mean and P-values were calculated using an unpaired T-test; and **(d)** RT-PCR analysis of

502 *BCL2* transcripts in fibroblasts following 2´O-methyl phosphorothioate AO transfection, as indicated at 100 and 50
503 nM (24 hours).
504
505 after 5 hours in two sister cells. Nuclear inclusions became larger and more compact
506 overtime, followed by caspase activation after 22 hours. No caspase activation was observed
507 in the absence of intranuclear inclusions, identifying nuclear inclusion as complicit in
508 caspase activated apoptosis, leading to cell death. The tumour suppressor protein p53 was
509 decreased, following transfection with 2´ O-methyl phosphorothioate AOs, relative to
510 untreated control cells (**Figure 5b and c**), suggesting that the cell death observed was p53
511 independent, contrary to the findings by Shen *et al.,* 2018 (Shen *et al.* 2018) when using a 2′
512 fluoro-modified AO on a phosphorothioate backbone in the mouse. In comparison to
513 phosphorothioate AO transfection, p53 levels remained unchanged following PMO
514 transfection (**Figure 5b and c**).
515
516 The mitochondrial membrane and apoptosis regulating, *BCL2*-like gene encodes two
517 alternatively spliced, functional protein isoforms, a longer anti-apoptotic isoform BCL-xL,
518 and a shorter pro-apoptotic isoform BCL-xS. Increased abundance of the BCL-xS isoform
519 induces cytochrome C release from the mitochondria, initiating caspase activated apoptosis.
520 RT-PCR across the *BCL* transcripts (**Figure 5d**) shows 2´ O-methyl phosphorothioate AO
521 transfection induces non-specific alternative splicing, increasing the levels of the pro-
522 apoptotic *BCL-xS* transcript, potentially initiating the caspase activation shown in **Figure 5a**.
523
524 *Transcriptome analysis of 2´ O-methyl phosphorothioate transfected cells reveals global*
525 *cellular disruptions*
526 We next evaluated the effect of 2´ O-methyl phosphorothioate transfection and nuclear
527 inclusion formation on the transcriptome by RNA-seq. We prepared RNA from fibroblasts
528 transfected with the two 2´ O-methyl phosphorothioate AOs used throughout this study as
529 well as two control samples (untreated cells and cells transfected with a DNA phosphodiester
530 AO (DNA control) version of the same sequence as the control AO, 100 nM for 24 hours) for
531 RNAseq analysis (n=3). The RNAseq data is available
532 at https://www.ncbi.nlm.nih.gov/geo/query/acc.cgi?acc=GSE121713 (accession number:
533 GSE121713). An RNAseq heatmap comparing the expression of transcripts in 2´ O-methyl
534 phosphorothioate AO transfected fibroblasts to that in cells transfected with the DNA
535 phosphodiester oligonucleotide and untreated cells showed stark differences in expression

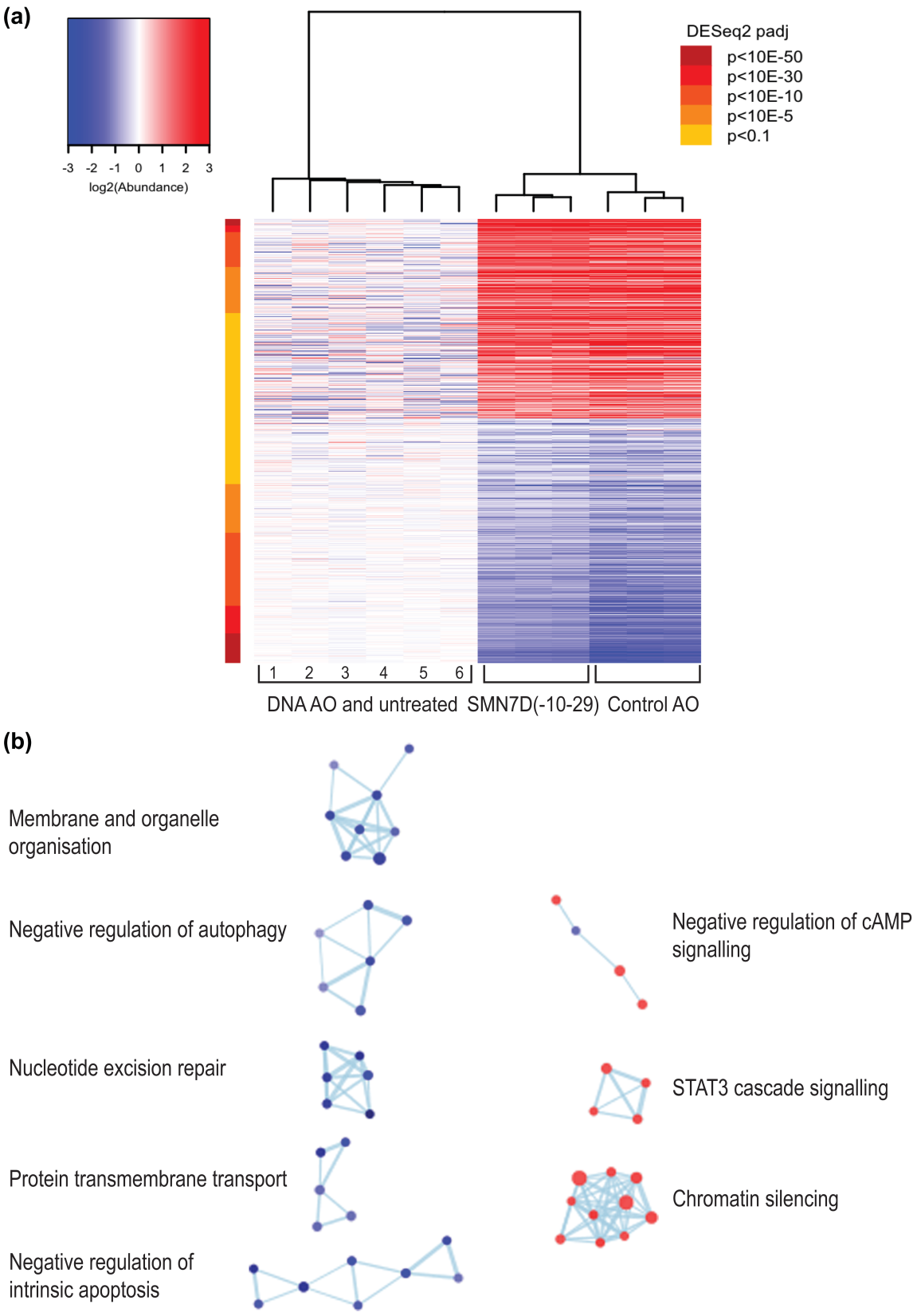

Figure 6 – RNA sequencing analysis of 2´ O-methyl phosphorothioate AO transfected fibroblasts. (a) heatmap of all differentially expressed transcripts in control (1, 4, 5-untreated and 2, 3, 6, DNA AO) and 2´ O-methyl phosphorothioate AO *SMN7D(-10-29)* and control AO) transfected (100 nM, 24 hours) cells, whereby red

541 represents overexpressed transcripts, and blue represents under-expressed transcripts; and **(b)** gene ontology
542 (GO) network of significantly affected cellular pathways in samples from transfected, compared to untreated and
543 DNA AO transfected cells. GO terms are represented as dots being either overexpressed (red) or under-
544 expressed (blue), and groups with greater than 50% of genes in common are linked.
545

546 between the groups (**Figure 6a**). Transcripts that are overexpressed in 2´ O-methyl
547 phosphorothioate AO transfected cells compared to controls are indicated in red, while those
548 that are underexpressed are indicated in blue.
549

550 Gene ontology (GO) analyses showed significant disruptions in transcripts involved in a
551 number of major cellular pathways. The GO network (**Figure 6b**) revealed cellular processes
552 and pathways that are significantly over-expressed include signaling pathways, chromatin
553 silencing, and metabolic pathways, while those that are significantly under-expressed
554 include negative regulation of apoptosis and autophagy, membrane and organelle
555 organisation, protein transmembrane transport and nucleotide excision repair. Gene ontology
556 pathways included in each cellular process are listed in **Supplementary File 2.** Thus, overall
557 these data show dramatic and widespread changes to gene expression in human fibroblasts
558 as a result of the uptake of the 2´ O-methyl phosphorothioate AOs.
559

560 **Discussion**

561 AOs have therapeutic potential as modulators of gene expression in many different diseases,
562 and can do so through several different mechanisms. Antisense drugs that are in current
563 clinical use alter exon selection during pre-mRNA processing, or induce RNaseH degradation
564 of the target mRNA, the mechanism of action determined by the nature of the AO chemistry
565 (for review see (Tri Le *et al.* 2016)). However, emerging reports of off-target effects
566 conferred by synthetic oligonucleotides, identified *in vitro* (Shen *et al.* 2014, Shen *et al.* 2015)
567 and *in vivo* (Shen *et al.* 2014, Shen *et al.* 2018), demand careful examination of the molecular
568 effects of these compounds. Here we report that transfection of cultured human dermal
569 fibroblasts, U2OS osteosarcoma cells, SH-SY5Y neuroblastoma cells and primary myogenic
570 cells with 2´ O-methyl phosphorothioate oligonucleotides causes the formation of large
571 structured nuclear inclusions, decorated with proteins that are normally components of
572 nuclear organelles, in particular, paraspeckles. We show evidence that 2´ O-methyl
573 phosphorothioate AO transfection alters the distribution of proteins normally associated with
574 subnuclear bodies, impacts on global transcript expression and ribosomal RNA processing,

575 among other critical cellular processes, and induces cell stress, followed by apoptosis.

576

577 Interaction of phosphorothioate oligonucleotides with nuclear proteins, including certain
578 paraspeckle proteins, and the formation of paraspeckle-like structures, independent of
579 *NEAT1,* has been reported (Shen *et al.* 2014, Shen *et al.* 2015, Shen *et al.* 2018). While Shen
580 *et al.* (Shen *et al.* 2014) focused on the effect of phosphorothioate AOs on NONO and
581 reported altered paraspeckle structure, this was in the context of AO-mediated modulation of
582 gene expression, not the broader cell biology. Other off-target effects and non-specific
583 binding of proteins, initiated by the negatively charged phosphorothioate backbone have
584 been reported elsewhere (Dias and Stein 2002, Winkler *et al.* 2010, Liang *et al.* 2015).
585 Hence, our experience and extensive research usage of AOs prompted further investigation of
586 the global consequences of 2´ O-methyl phosphorothioate AO transfection on cell biology,
587 showing many significant changes, as described above. In contrast, the transfection of
588 (charge-neutral) PMOs in the current study did not disrupt subnuclear structures, or result in
589 any alteration in the distribution or staining intensity of the nuclear proteins studied. This
590 result was reproducible using multiple delivery techniques, including high dose, uncomplexed
591 PMO transfection, transfection of PMO annealed to a DNA leash and complexed with
592 liposome reagent, as well as nucleofection. In comparison, all 2´ O-methyl phosphorothioate
593 AO sequences tested induced novel, structured intranuclear inclusions, revealed by
594 transmission electron microscopy to have amyloid aggregate-like appearance.

595

596 The nuclear inclusions observed in phosphorothioate transfected cells are associated with
597 altered nuclear architecture, disturbed gene expression and ultimately, apoptosis. While
598 formation of such large, and apparently irreversible structures would be expected to impact on
599 nuclear biology, the likely consequences of aberrant sequestration of paraspeckle and other
600 nuclear proteins on RNA processing and post transcriptional regulation are of prime concern.
601 Paraspeckles are dynamic, RNA-protein nuclear organelles that occur in the interchromatin
602 space in mammalian cells and are now known to contain over 40 different proteins associated
603 with one architectural long non-coding RNA, *NEAT1_2* (for review see (Fox *et al.* 2018)).
604 Observed in most cultured cells-other than various stem cells, and cells experiencing stress,
605 paraspeckles regulate gene expression through sequestration of proteins and RNAs (Fox *et al.*
606 2018), but are also implicated in microRNA biogenesis (Jiang *et al.* 2017). Paraspeckle
607 proteins can undergo rapid, but normally reversible aggregation from monomers to form

608 amyloid-like structures, seeded by *NEAT1_2*, and likely mediated through prion-like domains
609 that are enriched in uncharged polar amino acids (Lancaster *et al.* 2014). The mechanism by
610 which phosphorothioate oligonucleotides induce some paraspeckle proteins to form aberrant
611 aggregates is unknown, however, we do know that sub cellular localization and
612 phosphorothioate AO behaviour in transfected cells is influenced by protein interactions and
613 the 2´ sugar AO modifications (Bailey *et al.* 2017, Crooke *et al.* 2017), and that synthetic
614 double stranded RNA is also able to seed *de novo* paraspeckle formation (Shelkovnikova *et*
615 *al.* 2018). How other nuclear proteins become incorporated into the phosphorothioate AO
616 induced nuclear inclusions, and why TDP43, a major component of paraspeckles does not
617 appear in these inclusions in our study, remains elusive.
618
619 Immunofluorescent staining of 2´ O-methyl phosphorothioate transfected fibroblasts revealed
620 the paraspeckle components NONO, PSPC1, SFPQ and FUS co-localised with large nuclear
621 structures in excess of 2000 nm in length, with FUS decorating the structures in an ordered
622 manner. All four of these proteins include prion-like domains (for review see (Fox *et al.*
623 2018)) and we speculate that the known propensity of phosphorothioate backbone compounds
624 to interact with and bind proteins then alters the liquid-liquid phase properties of the
625 paraspeckle proteins, shifting them towards insoluble, amyloid-like aggregations. However,
626 not all paraspeckle components with prion-like domains investigated were found to colocalise
627 with the inclusions, and in addition, the localisation and distribution of some proteins
628 associated with other subnuclear bodies was altered in cells with nuclear inclusions.
629
630 Coilin, an integral component of Cajal bodies, nucleolin, one of the most abundant proteins in
631 the nucleolus but also found in the cytoplasm and on the cell membrane, fibrillarin, located in
632 the dense fibrillar component of the nucleolus and SC35 (SRSF2), an essential splicing factor
633 found in nuclear speckles all showed altered distribution in cells that have phosphorothioate
634 AO -induced nuclear inclusions, but did not co-localize with these inclusions. Cajal bodies
635 assemble spliceosomal and nucleolar ribonucleoproteins required for pre-mRNA and pre-
636 rRNA processing, and are recently proposed to contribute to genome organization, with global
637 effects on gene expression and RNA splicing (Wang *et al.* 2016). The nucleolus is the most
638 prominent nuclear structure, and is where synthesis and processing of ribosomal transcripts to
639 yield the mature rRNAs *5.8S, 18S* and *28S* from the *45S* pre- rRNA takes place. We show that
640 ribosomal RNA processing is greatly impaired by 2´ O-methyl phosphorothioate AO

641 transfection, and speculate that this is a likely manifestation of improper localization of major
642 protein components of the nucleolus and Cajal bodies and consequent disruption to their
643 functions. In addition, the aberrant inclusions that we speculate occupy interchromosomal
644 spaces may well impose physical constraints upon nuclear organisation, and prevent proper
645 localisation of Cajal bodies and the nucleoli close to their normal chromosomal sites. Tissues
646 with high demand for transcript splicing and ribosome biogenesis, and neurons in particular,
647 have prominent Cajal bodies, juxtaposed to nucleoli (for review see (Lafarga *et al.* 2017)),
648 and disruption or loss of Cajal bodies is associated with severe neuronal dysfunction (Tapia *et*
649 *al.* 2017). Indeed, disruption or depletion of Cajal bodies was seen as the earliest nuclear sign
650 of motor neuron degeneration in a spinal muscular atrophy mouse model and induced a
651 progressive nucleolar dysfunction in ribosome biogenesis (Tapia *et al.* 2017).
652
653 Paraspeckle biology has gained increasing interest due to the association of paraspeckle
654 proteins with neurodegenerative disease, in particular amyotrophic lateral sclerosis (ALS),
655 and the observation that *NEAT1_2* is up-regulated in early-stage motor neurons from the
656 spinal cords of ALS patients (Shelkovnikova *et al.* 2014, Yamazaki and Hirose 2015).
657 Paraspeckle formation, not observed in healthy spinal motor neurons, is enhanced in spinal
658 cords of patients with early stage sporadic and familial ALS, and mutations in many
659 paraspeckle proteins (eg. TDP-43, FUS, NONO, SFPQ) are associated with ALS (Nishimoto
660 *et al.* 2013, Shelkovnikova *et al.* 2018). Whether paraspeckles are protective or causative in
661 ALS molecular pathology is not known at this time (Yamazaki and Hirose 2015), nor is the
662 role of paraspeckles in disease well understood. Nevertheless, phosphorothioate AO-
663 mediated dysregulation of paraspeckle formation and altered nucleoli and Cajal body biology
664 shown in our study, together with the building body of evidence that nuclear organelle
665 dysfunction (Lafarga *et al.* 2017, Tapia *et al.* 2017) has implications for central nervous
666 system, and probably all, clinical applications of these compounds.
667
668 Not surprisingly, considering the altered nuclear architecture and distribution of proteins
669 implicated in RNA biology, transcriptome sequencing showed significant global effects on the
670 expression of transcripts and revealed disturbances to many critical cellular processes in
671 phosphorothioate AO transfected cells. Of particular concern, pathways involved in apoptosis,
672 chromatin silencing, cellular metabolism and a number of signalling pathways, autophagy and
673 nucleotide excision repair were disturbed. While we acknowledge that these *in vitro* studies in

674 replicating cells may not fully reflect potential off-target treatment effects in tissues *in vivo*,
675 Toonan et al., 2018 (Toonen *et al.* 2018) report significant upregulation of immune system-
676 associated genes in brains of mice treated by intracerebroventricular injection of 2′ O-methyl
677 phosphorothioate AO. The upregulation of immune system associated genes was detectable for
678 at least 2 months after the last AO administration. Here, the exaggerated sequestration of
679 nuclear proteins as a result of 2′ O-methyl phosphorothioate AO transfection dramatically
680 disturbs RNA processing, disrupts nuclear architecture, and induces apoptosis, and it seems
681 reasonable to consider that injection site reactions and adverse effects reported after clinical
682 evaluation of the 2′ O-methyl phosphorothioate *Drisapersen* for the treatment of Duchenne
683 muscular dystrophy (Mendell *et al.* 2017) and *Kynamro*® (*Mipomersen*) for the treatment of
684 familial hypercholesterolemia (Wong and Goldberg 2014) may be mediated at least in part, by
685 non-specific interactions of nuclear components with the AO backbone. It might also be
686 prudent to deliberate on the reported effects of antisense drugs, attributed to the AO action on
687 the target transcript, and consider whether some level of the apparent antisense effect on
688 splicing, in particular, could perhaps be a consequence of disturbance of RNA processing
689 pathways more broadly.
690
691 We speculate that, unlike endogenous paraspeckles and other dynamic nuclear bodies, the
692 formation of the aberrant nuclear inclusions seen *in vitro* here does not appear to be
693 reversible. While 2′ O-methyl phosphorothioate transfected cultures showed reduced cell
694 numbers, whether this was due to cell death or impaired replication, or both, is uncertain, and
695 whether the nuclear inclusions *per se* or reduced availability of RNA processing are primarily
696 responsible requires further investigation. However, any effects resulting in perturbation of
697 nuclear proteins may be compounded by the formation of the nuclear amyloid-like
698 aggregates and likely disturbance of protein homeostasis, termed 'proteostasis' (Yerbury *et*
699 *al.* 2016). Although other descriptions of exogenously induced nuclear amyloid-like
700 aggregates are limited, Arnhold *et al.,* 2015 (Arnhold *et al.* 2015) identified large amyloid-
701 like aggregates in SH-SY5Y cells, treated with mercury, a notorious neurotoxicant, in a study
702 that explains the mechanism of heavy metal neurotoxicity and identified amyloid protein
703 aggregation in the cell nucleus as causative. Mass spectrometry of the purified protein
704 aggregates identified a subset of spliceosomal components and the nuclear envelope protein
705 lamin B1 (Arnhold *et al.* 2015). In our study, we also detected changes in lamin B1, although
706 here we did not detect lamin B1 in the nuclear inclusions, we nevertheless observed that

707 nuclear membrane and lamin B1 organization was distorted in fibroblasts containing nuclear
708 inclusions. Interestingly, the multi-lobulated nuclei and lamin B1 staining are reminiscent of
709 cells from progeria patients carrying the lamin A 433G>A mutation (E145K) (Taimen *et al.*
710 2009).
711

712 In summary, we report phosphorothioate backbone-specific effects of modified
713 oligonucleotides on the distribution and localization of nuclear proteins, appearance of novel
714 nuclear structures composed in part of a subset of paraspeckle protein components, and
715 sequence-independent effects on nascent RNA processing. While the *in vivo,* longer term
716 repercussions of exogenous oligonucleotide-induced nuclear protein aggregates that include
717 many paraspeckle components and cause sub-nuclear disorganisation are yet to be
718 determined, our observations suggest that phosphorothioate backbone antisense compounds
719 destined for clinical application would benefit from further scrutiny.
720

721 **Acknowledgments**
722 The authors would like to acknowledge technical advice from Russell Johnsen. This work was
723 performed in part during LLF's and ILP's PhD candidatures. Laboratory studies and ILP were
724 supported by funding from the Parry Foundation through the Spinal Muscular Atrophy
725 Association of Australia and LLF received a Team Spencer and Muscular Dystrophy WA PhD
726 stipend. The authors received research support from the NHMRC Project Grants
727 APP1147496, APP1086311, APP1144791 and the MNDi foundation, Western Australia.
728

729 **Author Contributions**
730 Conceived and designed experiments: LLF, RL, SF, MTA, ILP and AF. Performed
731 experiments: LLF, RL, MTA, ILP, AH, and LG. Analysis of RNA-seq data: JC. Prepared and
732 edited manuscript: LLF, SF, RL, MTA, ILP, JC, AH, LG, SDW and AF.
733 Declaration of interests: SF and SDW act as consultants to Sarepta Therapeutics and are
734 named inventors of patents licensed through the University of Western Australia to Sarepta
735 Therapeutics. As such, they are entitled to milestone and royalty payments that may be
736 generated from licensing agreements and are involved in ongoing collaborative research
737 projects with Sarepta Therapeutics.
738
739
740

741 **References:**
742 AM Adams, PL Harding, PL Iversen, C Coleman, S Fletcher and SD Wilton (2007).
743 **Antisense oligonucleotide induced exon skipping and the dystrophin gene**
744 **transcript: Cocktails and chemistries**. *BMC Mol Biol* **8**: 57
745
746 F Arnhold, KH Guhrs and A von Mikecz (2015). **Amyloid domains in the cell nucleus**
747 **controlled by nucleoskeletal protein lamin b1 reveal a new pathway of mercury**
748 **neurotoxicity**. *PeerJ* **3**: e754.10.7717/peerj.754

JK Bailey, W Shen, XH Liang and ST Crooke (2017). **Nucleic acid binding proteins affect the subcellular distribution of phosphorothioate antisense oligonucleotides**. *Nucleic Acids Res* **45**(18): 10649-10671.10.1093/nar/gkx709

CF Bennett, BF Baker, N Pham, E Swayze and RS Geary (2017). **Pharmacology of antisense drugs**. *Annu Rev Pharmacol Toxicol* **57**: 81-105.10.1146/annurev-pharmtox-010716-104846

CS Bond and AH Fox (2009). **Paraspeckles: Nuclear bodies built on long noncoding rna**. *J Cell Biol* **186**(5): 637-644.10.1083/jcb.200906113

M Chakravarthy, S Chen, PR Dodd and RN Veedu (2017). **Nucleic acid-based theranostics for tackling alzheimer's disease**. *Theranostics* **7**(16): 3933-3947.10.7150/thno.21529

ST Crooke, S Wang, TA Vickers, W Shen and XH Liang (2017). **Cellular uptake and trafficking of antisense oligonucleotides**. *Nat Biotechnol* **35**(3): 230-237.10.1038/nbt.3779

N Dias and CA Stein (2002). **Potential roles of antisense oligonucleotides in cancer therapy. The example of bcl-2 antisense oligonucleotides**. *Eur J Pharm Biopharm* **54**(3): 263-269

S Fletcher, K Honeyman, AM Fall, PL Harding, RD Johnsen and SD Wilton (2006). **Dystrophin expression in the mdx mouse after localised and systemic administration of a morpholino antisense oligonucleotide**. *J Gene Med* **8**(2): 207-216

U Flierl, TL Nero, B Lim, JF Arthur, Y Yao, SM Jung, E Gitz, AY Pollitt, MT Zaldivia, M Jandrot-Perrus, A Schafer, B Nieswandt, RK Andrews, MW Parker, EE Gardiner and K Peter (2015). **Phosphorothioate backbone modifications of nucleotide-based drugs are potent platelet activators**. *J Exp Med* **212**(2): 129-137.10.1084/jem.20140391

AH Fox, S Nakagawa, T Hirose and CS Bond (2018). **Paraspeckles: Where long noncoding rna meets phase separation**. *Trends Biochem Sci* **43**(2): 124-135.10.1016/j.tibs.2017.12.001

BL Gebski, CJ Mann, S Fletcher and SD Wilton (2003). **Morpholino antisense oligonucleotide induced dystrophin exon 23 skipping in mdx mouse muscle**. *Hum Mol Genet* **12**(15): 1801-1811

L Jiang, C Shao, QJ Wu, G Chen, J Zhou, B Yang, H Li, LT Gou, Y Zhang, Y Wang, GW Yeo, Y Zhou and XD Fu (2017). **Neat1 scaffolds rna-binding proteins and the microprocessor to globally enhance pri-mirna processing**. *Nat Struct Mol Biol* **24**(10): 816-824.10.1038/nsmb.3455

M Kinali, V Arechavala-Gomeza, L Feng, S Cirak, D Hunt, C Adkin, M Guglieri, E Ashton, S Abbs, P Nihoyannopoulos, ME Garralda, M Rutherford, C McCulley, L Popplewell, IR Graham, G Dickson, MJ Wood, DJ Wells, SD Wilton, R Kole, V Straub, K Bushby, C Sewry, JE Morgan and F Muntoni (2009). **Local restoration of dystrophin expression with the morpholino oligomer avi-4658 in duchenne muscular dystrophy: A single-**

blind, placebo-controlled, dose-escalation, proof-of-concept study. *Lancet Neurol* **8**(10): 918-928.S1474-4422(09)70211-X [pii] 10.1016/S1474-4422(09)70211-X

M Lafarga, O Tapia, AM Romero and MT Berciano (2017). **Cajal bodies in neurons**. *RNA Biol* **14**(6): 712-725.10.1080/15476286.2016.1231360

AK Lancaster, A Nutter-Upham, S Lindquist and OD King (2014). **Plaac: A web and command-line application to identify proteins with prion-like amino acid composition**. *Bioinformatics* **30**(17): 2501-2502.10.1093/bioinformatics/btu310

R Li, AR Harvey, SI Hodgetts and AH Fox (2017). **Functional dissection of neat1 using genome editing reveals substantial localization of the neat1_1 isoform outside paraspeckles**. *RNA* **23**(6): 872-881.10.1261/rna.059477.116

S Li, FJ Shu, Z Li, L Jaafar, S Zhao and WS Dynan (2017). **Cell-type specific role of the rna-binding protein, nono, in the DNA double-strand break response in the mouse testes**. *DNA Repair (Amst)* **51**: 70-78.10.1016/j.dnarep.2017.02.002

XH Liang, H Sun, W Shen and ST Crooke (2015). **Identification and characterization of intracellular proteins that bind oligonucleotides with phosphorothioate linkages**. *Nucleic Acids Res* **43**(5): 2927-2945.10.1093/nar/gkv143

F Lipi, S Chen, M Chakravarthy, S Rakesh and RN Veedu (2016). **In vitro evolution of chemically-modified nucleic acid aptamers: Pros and cons, and comprehensive selection strategies**. *RNA Biol* **13**(12): 1232-1245.10.1080/15476286.2016.1236173

JR Mendell, N Goemans, LP Lowes, LN Alfano, K Berry, J Shao, EM Kaye, E Mercuri, G Eteplirsen Study and DMDIN Telethon Foundation (2016). **Longitudinal effect of eteplirsen versus historical control on ambulation in duchenne muscular dystrophy**. *Ann Neurol* **79**(2): 257-271.10.1002/ana.24555

JR Mendell, LR Rodino-Klapac, Z Sahenk, K Roush, L Bird, LP Lowes, L Alfano, AM Gomez, S Lewis, J Kota, V Malik, K Shontz, CM Walker, KM Flanigan, M Corridore, JR Kean, HD Allen, C Shilling, KR Melia, P Sazani, JB Saoud, EM Kaye and G Eteplirsen Study (2013). **Eteplirsen for the treatment of duchenne muscular dystrophy**. *Ann Neurol* **74**(5): 637-647.10.1002/ana.23982

JR Mendell, Z Sahenk and L Rodino-Klapac (2017). **Clinical trials of exon skipping in duchenne muscular dystrophy**. *Expert Opinion on Orphan Drugs* **5**(9): 683-690.DOI: 10.1080/21678707.2017.1366310

C Mitrpant, P Porensky, H Zhou, L Price, F Muntoni, S Fletcher, SD Wilton and AH Burghes (2013). **Improved antisense oligonucleotide design to suppress aberrant smn2 gene transcript processing: Towards a treatment for spinal muscular atrophy**. *PLoS One* **8**(4): e62114.10.1371/journal.pone.0062114

T Naganuma, S Nakagawa, A Tanigawa, YF Sasaki, N Goshima and T Hirose (2012). **Alternative 3'-end processing of long noncoding rna initiates construction of nuclear paraspeckles**. *EMBO J* **31**(20): 4020-4034.10.1038/emboj.2012.251

Y Nishimoto, S Nakagawa, T Hirose, HJ Okano, M Takao, S Shibata, S Suyama, K Kuwako, T Imai, S Murayama, N Suzuki and H Okano (2013). **The long non-coding rna nuclear-enriched abundant transcript 1_2 induces paraspeckle formation in the motor neuron during the early phase of amyotrophic lateral sclerosis**. *Mol Brain* **6**: 31.10.1186/1756-6606-6-31

DM Paton (2017). **Nusinersen: Antisense oligonucleotide to increase smn protein production in spinal muscular atrophy**. *Drugs Today (Barc)* **53**(6): 327-337.10.1358/dot.2017.53.6.2652413

TA Shelkovnikova, MS Kukharsky, H An, P Dimasi, S Alexeeva, O Shabir, PR Heath and VL Buchman (2018). **Protective paraspeckle hyper-assembly downstream of tdp-43 loss of function in amyotrophic lateral sclerosis**. *Mol Neurodegener* **13**(1): 30.10.1186/s13024-018-0263-7

TA Shelkovnikova, HK Robinson, C Troakes, N Ninkina and VL Buchman (2014). **Compromised paraspeckle formation as a pathogenic factor in fusopathies**. *Human Molecular Genetics* **23**(9): 2298-2312.10.1093/hmg/ddt622

L Shen, A Frazer-Abel, PR Reynolds, PC Giclas, A Chappell, MK Pangburn, H Younis and SP Henry (2014). **Mechanistic understanding for the greater sensitivity of monkeys to antisense oligonucleotide-mediated complement activation compared with humans**. *J Pharmacol Exp Ther* **351**(3): 709-717.10.1124/jpet.114.219378

W Shen, CL De Hoyos, H Sun, TA Vickers, XH Liang and ST Crooke (2018). **Acute hepatotoxicity of 2' fluoro-modified 5-10-5 gapmer phosphorothioate oligonucleotides in mice correlates with intracellular protein binding and the loss of dbhs proteins**. *Nucleic Acids Res* **46**(5): 2204-2217.10.1093/nar/gky060

W Shen, XH Liang and ST Crooke (2014). **Phosphorothioate oligonucleotides can displace neat1 rna and form nuclear paraspeckle-like structures**. *Nucleic Acids Res* **42**(13): 8648-8662.10.1093/nar/gku579

W Shen, XH Liang, H Sun and ST Crooke (2015). **2'-fluoro-modified phosphorothioate oligonucleotide can cause rapid degradation of p54nrb and psf**. *Nucleic Acids Res* **43**(9): 4569-4578.10.1093/nar/gkv298

NK Singh, NN Singh, EJ Androphy and RN Singh (2006). **Splicing of a critical exon of human survival motor neuron is regulated by a unique silencer element located in the last intron**. *Mol Cell Biol* **26**(4): 1333-1346.10.1128/MCB.26.4.1333-1346.2006

CA Stein and D Castanotto (2017). **Fda-approved oligonucleotide therapies in 2017**. *Mol Ther* **25**(5): 1069-1075.10.1016/j.ymthe.2017.03.023

P Taimen, K Pfleghaar, T Shimi, D Moller, K Ben-Harush, MR Erdos, SA Adam, H Herrmann, O Medalia, FS Collins, AE Goldman and RD Goldman (2009). **A progeria mutation reveals functions for lamin a in nuclear assembly, architecture, and chromosome organization**. *Proc Natl Acad Sci U S A* **106**(49): 20788-20793.10.1073/pnas.0911895106

O Tapia, JO Narcis, J Riancho, O Tarabal, L Piedrafita, J Caldero, MT Berciano and M Lafarga (2017). **Cellular bases of the rna metabolism dysfunction in motor neurons of a murine model of spinal muscular atrophy: Role of cajal bodies and the nucleolus**. *Neurobiol Dis* **108**: 83-99.10.1016/j.nbd.2017.08.004

LJA Toonen, J Casaca-Carreira, M Pellise-Tintore, H Mei, Y Temel, A Jahanshahi and WMC van Roon-Mom (2018). **Intracerebroventricular administration of a 2'-o-methyl phosphorothioate antisense oligonucleotide results in activation of the innate immune system in mouse brain**. *Nucleic Acid Ther* **28**(2): 63-73.10.1089/nat.2017.0705

B Tri Le, RN Veedu, S Fletcher and SD Wilton (2016). **Antisense oligonucleotide development for the treatment of muscular dystrophies**. *Expert Opinion on Orphan Drugs* **4**(2): 139-152.10.1517/21678707.2016.1122517

RN Veedu (2015). **Medicinal chemistry of aptamers**. *Curr Top Med Chem* **15**(12): 1065

Q Wang, IA Sawyer, MH Sung, D Sturgill, SP Shevtsov, G Pegoraro, O Hakim, S Baek, GL Hager and M Dundr (2016). **Cajal bodies are linked to genome conformation**. *Nat Commun* **7**: 10966.10.1038/ncomms10966

SD Wilton, RN Veedu and S Fletcher (2015). **The emperor's new dystrophin: Finding sense in the noise**. *Trends Mol Med* **21**(7): 417-426.10.1016/j.molmed.2015.04.006

J Winkler, M Stessl, J Amartey and CR Noe (2010). **Off-target effects related to the phosphorothioate modification of nucleic acids**. *ChemMedChem* **5**(8): 1344-1352.10.1002/cmdc.201000156

E Wong and T Goldberg (2014). **Mipomersen (kynamro): A novel antisense oligonucleotide inhibitor for the management of homozygous familial hypercholesterolemia**. *P T* **39**(2): 119-122

T Yamazaki and T Hirose (2015). **The building process of the functional paraspeckle with long non-coding rnas**. *Front Biosci (Elite Ed)* **7**: 1-41

JJ Yerbury, L Ooi, A Dillin, DN Saunders, DM Hatters, PM Beart, NR Cashman, MR Wilson and H Ecroyd (2016). **Walking the tightrope: Proteostasis and neurodegenerative disease**. *Journal of Neurochemistry* **137**(4): 489-505.10.1111/jnc.13575